AGU PUBLICATIONS

JGR

Journal of Geophysical Research: Atmospheres

RESEARCH ARTICLE
10.1002/2015JD024737

Evaluating N_2O_5 heterogeneous hydrolysis parameterizations for CalNex 2010

Wayne L. Chang[1], Steven S. Brown[2], Jochen Stutz[3], Ann M. Middlebrook[2], Roya Bahreini[4], Nicholas L. Wagner[2], William P. Dubé[2], Ilana B. Pollack[5], Thomas B. Ryerson[2], and Nicole Riemer[1]

[1]Department of Atmospheric Sciences, University of Illinois at Urbana-Champaign, Urbana, Illinois, USA, [2]Chemical Sciences Division, Earth System Research Laboratory, NOAA, Boulder, Colorado, USA, [3]Department of Atmospheric and Oceanic Sciences, University of California, Los Angeles, California, USA, [4]Department of Environmental Sciences, University of California, Riverside, California, USA, [5]Department of Atmospheric Science, Colorado State University, Fort Collins, Colorado, USA

Key Points:
- Evaluated parameterizations of N_2O_5 heterogeneous hydrolysis for CalNex 2010 using WRF-Chem
- N_2O_5 uptake coefficient parameterization has noticeable impact on NO_x and ozone predictions
- Improved closure for modeled and observed uptake coefficients when including organic coatings

Supporting Information:
- Supporting Information S1
- Figure S1
- Figure S2
- Figure S3
- Figure S4

Correspondence to:
N. Riemer,
nriemer@illinois.edu

Citation:
Chang, W. L., S. S. Brown, J. Stutz, A. M. Middlebrook, R. Bahreini, N. L. Wagner, W. P. Dubé, I. B. Pollack, T. B. Ryerson, and N. Riemer (2016), Evaluating N_2O_5 heterogeneous hydrolysis parameterizations for CalNex 2010, *J. Geophys. Res. Atmos.*, *121*, 5051–5070, doi:10.1002/2015JD024737.

Received 31 DEC 2015
Accepted 16 APR 2016
Accepted article online 23 APR 2016
Published online 7 MAY 2016

Abstract Nighttime chemistry in the troposphere is closely tied to the dinitrogen pentoxide (N_2O_5) budget, but high uncertainties remain regarding the model representation of the heterogeneous hydrolysis of N_2O_5 on aerosol particles. In this study we used the community model WRF-Chem to simulate a 3-day period during the California Nexus (CalNex) Campaign in 2010. We extended WRF-Chem to include the heterogeneous hydrolysis of N_2O_5 and contrasted the impact of different published parameterizations of N_2O_5 heterogeneous hydrolysis on the spatial distribution of uptake coefficients and the resulting N_2O_5 concentrations. For all the cases, modeled N_2O_5 uptake coefficients showed strong spatial variability, with higher values in the nocturnal boundary layer compared to the residual layer, especially in environments with high relative humidities, such as over the ocean and along the coast. The best agreement of modeled and observed uptake coefficients was obtained using the parameterization by Davis et al. (2008) combined with the treatment of organic coating by Riemer et al. (2009). For this case the temporal evolution of lower boundary layer N_2O_5 mixing ratios was reproduced well, and the predictions of surface mixing ratios of ozone and NO_x were improved. However, the model still overpredicted the uptake coefficients in the residual layer and consequently underpredicted N_2O_5 concentrations in the residual layer. This study also highlights that environments with low relative humidities pose a challenge for aerosol thermodynamic models in calculating aerosol water uptake, and this impacts N_2O_5 heterogeneous hydrolysis parameterizations.

1. Introduction

Dinitrogen pentoxide (N_2O_5) is a nighttime reservoir for NO_x (NO_x = NO + NO_2). In the troposphere N_2O_5 concentrations exhibit a unique vertical profile with maximum values located near the top of the stable nighttime boundary layer, as shown by both ambient measurements [*Brown et al.*, 2007a, 2007b; *Stutz et al.*, 2004] and model simulations [*Galmarini et al.*, 1997; *Riemer et al.*, 2003; *Geyer and Stutz*, 2004]. N_2O_5 accumulates in elevated layers at night, rather than near the surface, because fresh emissions of NO and volatile organic compounds (VOC) titrate the N_2O_5 precursors, O_3, and NO_3.

The main loss pathway of N_2O_5 is its heterogeneous hydrolysis on aerosol particles [*Russell et al.*, 1985; *Hanway and Tao*, 1998]. Removal of N_2O_5 in the troposphere is also an indirect loss pathway of NO_x and NO_3, which impacts both the daytime and nighttime oxidative capacity of the troposphere [*Dentener and Crutzen*, 1993; *Brown et al.*, 2011; *Young et al.*, 2012] as well as the regional and global aerosol budget [*Riemer et al.*, 2003; *Pathak et al.*, 2011; *Macintyre and Evans*, 2010]. The formation of nitric acid (HNO_3) by N_2O_5 heterogeneous hydrolysis is not only an efficient sink for NO_x but also a key contributor to the nitrate aerosol loading. This applies especially during winter, when the conditions are favorable for both N_2O_5 formation and for the partitioning of HNO_3 into the particle phase [*Pathak et al.*, 2011; *Kim et al.*, 2014].

In addition to nitric acid, the N_2O_5 heterogeneous reaction may produce a chlorine radical precursor, nitryl chloride ($ClNO_2$) [*Thornton et al.*, 2010], which has been widely observed in different environments [*Mielke et al.*, 2011; *Wagner et al.*, 2012; *Phillips et al.*, 2012]. During daytime $ClNO_2$ photolyzes to form the chlorine radical, which is known to impact the oxidizing power of the troposphere. *Sarwar et al.* [2012, 2014] examined

the impact of heterogeneous $ClNO_2$ production across the United States and the Northern Hemisphere and saw an enhancement of ozone levels in polluted regions, for both the winter and the summer seasons.

There are several factors that govern the N_2O_5 heterogeneous uptake reaction rate, some of which are related to meteorological conditions, others to the chemical composition of the aerosol population [*Chang et al.*, 2011]. High relative humidities and low temperatures promote N_2O_5 heterogeneous reaction on particles, while the presence of nitrate and organic species in the aerosol inhibits the N_2O_5 uptake. A key parameter to quantify the heterogeneous hydrolysis reaction rate is the uptake coefficient for N_2O_5 on aerosol particles.

Laboratory studies demonstrate that the N_2O_5 uptake coefficient γ can vary by several orders of magnitude [*Davis et al.*, 2008], depending on temperature, relative humidity, and aerosol composition. Hence, to assess the impact of N_2O_5 heterogeneous hydrolysis on atmospheric chemistry, an adequate model parameterization for γ is crucial. Several model studies have investigated the impact of N_2O_5 hydrolysis using parameterizations for γ that varied in complexity [e.g., *Evans and Jacob*, 2005; *Davis et al.*, 2008; *Riemer et al.*, 2009; *Bertram and Thornton*, 2009]. Overall, models tend to overpredict the observed values for the uptake coefficient [*Brown et al.*, 2009; *Riedel et al.*, 2012]; however, the opposite has been found by *Morgan et al.* [2015] for a study in northwestern Europe.

Our goal for this study is to contrast and evaluate state-of-the-art parameterizations of N_2O_5 heterogeneous hydrolysis. In particular, we unify the treatment of hydrolysis suppression due to nitrate and organic coatings by combining the parameterization for γ by *Davis et al.* [2008] to represent the inorganic core with the organic coating treatment by *Riemer et al.* [2009]. Similarly, we also examine a parameterization that combines the treatment for γ by *Bertram and Thornton* [2009] with the organic coating treatment by *Riemer et al.* [2009].

We compare the different parameterizations to each other using the community chemistry transport model WRF-Chem and compare the model results with observations from a major measurement campaign, the CalNex 2010 field campaign in Southern California [*Ryerson et al.*, 2013]. The CalNex data set is particularly suitable because it provides observations not only from ground sites but also from nighttime flights that captured the spatial distribution of N_2O_5 mixing ratios within the South Coast Air Basin of California (SoCAB).

2. Methods

2.1. N_2O_5 Chemical Reactions

The fate and impacts of N_2O_5 from the perspectives of laboratory experiments, ambient measurements, and model simulations have been summarized in *Chang et al.* [2011]. In short, the most important reactions involving N_2O_5 are as follows: The nitrate radical NO_3 is formed by the reaction of ozone and NO_2,

$$NO_2 + O_3 \longrightarrow NO_3 + O_2 \tag{1}$$

During nighttime, in the absence of photolysis reactions, NO_3 can accumulate and react with VOC. Additionally, NO_2 and NO_3 can react to form N_2O_5,

$$NO_2 + NO_3 + M \longleftrightarrow N_2O_5 + M \tag{2}$$

N_2O_5 is thermally unstable and can readily dissociate into NO_2 and NO_3. The N_2O_5 concentration is therefore highly dependent on temperature, where the equilibrium constant for reaction (2) can be approximated as a function of temperature alone.

The most important loss for N_2O_5 is the heterogeneous hydrolysis reaction, which produces HNO_3:

$$N_2O_{5(g)} + H_2O_{(aq)} \longrightarrow 2HNO_{3(aq)} \tag{3}$$

In the presence of particulate chloride, the N_2O_5 heterogeneous reaction can also produce $ClNO_2$:

$$N_2O_{5(g)} + Cl^-_{(aq)} \longrightarrow ClNO_{2(g)} + NO^-_{3(aq)} \tag{4}$$

In the present work, we consider only the production of nitric acid through this heterogeneous uptake, and the role of nitryl chloride production will be presented elsewhere.

The heterogeneous reaction can be modeled as a first-order loss of N_2O_5,

$$\frac{d[N_2O_5]}{dt} = -k_{N_2O_5}[N_2O_5]. \quad (5)$$

The loss rate constant, $k_{N_2O_5}$, is a function of mean molecular velocity of N_2O_5 ($c_{N_2O_5}$), available aerosol surface area density (S), and uptake coefficient (γ),

$$k_{N_2O_5} = \frac{1}{4} c_{N_2O_5} \cdot S \cdot \gamma. \quad (6)$$

Since the production of N_2O_5 is tied to the abundance of NO_3, and NO_3 is also consumed by reactions with VOC, the sensitivity of NO_x and O_3 toward γ depends on the NO_3 reaction rates with VOC. Specifically, if NO_3 reactivity with respect to reactions with VOC is very high, only little N_2O_5 is formed and the sensitivity of NO_x and O_3 toward γ is reduced.

The model representation of the uptake coefficient γ is described in the following section 2.2, and the method to derive γ based on field observations of trace gases concentrations is shown in section 2.3. We evaluate closure between the two in section 3.4.

2.2. Parameterization Techniques for the N_2O_5 Uptake Coefficient

To account for the impact of aerosol composition on heterogeneous N_2O_5 hydrolysis in our model simulations, we use the γ parameterization by *Riemer et al.* [2009]:

$$\gamma = \left(\frac{1}{\gamma_{core}} + \frac{1}{\gamma_{coat}} \right)^{-1}, \quad (7)$$

where the core of the particle is assumed to be inorganic, and the coating to be organic when both components are present in the aerosol mixture. We assume that all organic material (primary and secondary) contributes to the coating. This parameterization is an extension of the resistor model, where the presence of the coating limits the dissolution, diffusion and chemical reaction of N_2O_5 in particles. Evidence for the liquid-liquid phase separation in atmospheric particles has been documented by *You et al.* [2012], where organic and aqueous separations within aerosol particles were observed. This represents an upper limit for estimating the effect of an organic coating, because not all organic material necessarily contributes to the coating.

For γ_{core}, we compare two formulations: a statistically derived parametric fit based on a review of past chamber experiments by *Davis et al.* [2008], and the method by *Bertram and Thornton* [2009] that takes into account the presence of particulate chloride. The parameterization of γ_{core} by *Davis et al.* [2008] is defined by

$$\gamma^D_{core} = \sum_i x_i \gamma^*_i \quad (8)$$

where i represents the aerosol species NH_4HSO_4, $(NH_4)_2SO_4$, and NH_4NO_3, x_i represents the molar concentration of component i normalized by the total concentration of the three components combined, and γ^*_i is the corresponding statistical parameterization of component i constrained to be no greater than the maximum observed values based on laboratory experiments. For the details of the formulation of γ^*_i, please see *Davis et al.* [2008]. To summarize briefly, the coefficients γ^*_i are generally functions temperature and of relative humidity (RH). We used the statistical fits without the data by *Kane et al.* [2001], which means that the γ^*_i values for sulfate particles increase for RHs below 46% and are independent of RH above 46%. It is also important to note that the statistical fits based on the laboratory data yielded an RH dependence for dry aerosol. *Davis et al.* [2008] explained that this counterintuitive result may be due to an increase in surface-adsorbed water.

Since the Davis parameterization uses equation (8) to determine the overall uptake coefficient for a mixed aerosol, it inherently assumes that the particles are externally mixed with respect to sulfate and nitrate, thus not permitting as large a nitrate effect as is possible. It also assumes that subsets of the population can retain water based on different efflorescence RHs between the subpopulations of aerosol that may or may not reflect reality.

Table 1. Summary of Scenarios in This Study

Scenario Name	Aqueous Core Treatment	Organic Coating Treatment	Symbol
Base	None	None	-
Davis	*Davis et al.* [2008]	None	γ^{D}_{core}
B&T	*Bertram and Thornton* [2009]	None	γ^{B}_{core}
Davis+coat	*Davis et al.* [2008]	*Riemer et al.* [2009]	γ^{D}
B&T+coat	*Bertram and Thornton* [2009]	*Riemer et al.* [2009]	γ^{B}

The parameterization of γ^{B}_{core} by *Bertram and Thornton* [2009] is defined as

$$\gamma^{B}_{core} = Ak' \left(1 - \frac{1}{\left(\frac{k_3[H_2O(l)]}{k_{2b}[NO_3^-]}\right) + 1 + \left(\frac{k_4[Cl^-]}{k_{2b}[NO_3^-]}\right)} \right) \tag{9}$$

where $A = 3.2 \times 10^{-8}$ is an empirical prefactor, $H_2O(l)$ is particle liquid water, NO_3^- is particulate nitrate, Cl^- is particulate chloride, $k_3/k_{2b} = 6 \times 10^{-2}$, $k_4/k_{2b} = 29$, and k' can be calculated by

$$k' = \beta - \beta e^{(-\delta[H_2O](l))}. \tag{10}$$

Here $\beta = 1.15 \times 10^6$ s^{-1}, and $\delta = 1.3 \times 10^{-1}$ M^{-1}. In contrast to the Davis parameterization, this is inherently an internally mixed parameterization of the uptake coefficient. The nitrate effect is permitted to decrease the uptake coefficient at low water concentrations as one would expect based on laboratory results. The aerosol liquid water content needs to be provided by the aerosol thermodynamics model, which can be a challenging task as we will see later.

The treatment of organic coating is based on the work by *Riemer et al.* [2009],

$$\gamma_{coat} = \frac{4RTH_{org}D_{org}R_c}{c_{N_2O_5}} \cdot \ell \cdot R_p \tag{11}$$

where R is the universal gas constant, T is the temperature, H_{org} is the Henry's law constant of N_2O_5 for the organic coating, D_{org} is the diffusion coefficient of N_2O_5 in the organic coating, and R_p, R_c, and ℓ are the radius of the particle, the radius of the core, and the thickness of the coating, respectively. As in *Riemer et al.* [2009], for the product $D_{org}H_{org}$ we use values that are consistent with the analysis presented by *Anttila et al.* [2006] who showed that $D_{org}H_{org}$ is about $0.03D_{aq}H_{aq}$ for organic coatings consisting of condensed monoterpene oxidation products. Here H_{aq} is the Henry's law constant of N_2O_5 for the aqueous phase ($H_{aq} = 5000$ M atm^{-1}) and D_{aq} is the diffusion coefficient of N_2O_5 in the aqueous phase ($D_{aq} = 10^{-9}$ m^2 s^{-1}).

For the assessment of the parameterization methods discussed previously, we developed five test scenarios, as summarized in Table 1: "Base": no hydrolysis; "Davis": hydrolysis based on *Davis et al.* [2008]; "B&T": hydrolysis based on *Bertram and Thornton* [2009]; "Davis+coat": hydrolysis based on *Davis et al.* [2008], combined with the treatment of organic coating by *Riemer et al.* [2009]; "B&T+coat": hydrolysis based on *Bertram and Thornton* [2009], combined with the treatment of organic coating by *Riemer et al.* [2009]. We compare and contrast the simulated uptake coefficients and N_2O_5 mixing ratios resulting from these scenarios in section 3.3.

2.3. Uptake Coefficient Calculations Based on Observations

Brown et al. [2003] described how to derive uptake coefficients of N_2O_5 based on measurements of mixing ratios of N_2O_5, NO_3, NO_2, O_3, ambient temperature, and aerosol surface area density [*Brown et al.*, 2006; *Aldener et al.*, 2006]. An underlying assumption of this analysis is that N_2O_5, NO_3, and NO_2 are in steady state. To derive these "steady state uptake coefficients" (γ_{ss}), data sets from flight segments of several minutes duration are used. The validity of the steady state approximation was checked against a box model calculation using the derived loss rate coefficients for NO_3 and N_2O_5 together with ambient temperature, average NO_2 and O_3 mixing ratios for each flight segment.

Steady state lifetimes (τ) are defined as the ratio of the concentration (or mixing ratio) of NO_3, N_2O_5, or their sum ($NO_3 + N_2O_5$) to their production through the oxidation of NO_2 by ozone:

$$\tau_{NO_3} = \frac{[NO_3]}{k[O_3][NO_2]} \tag{12}$$

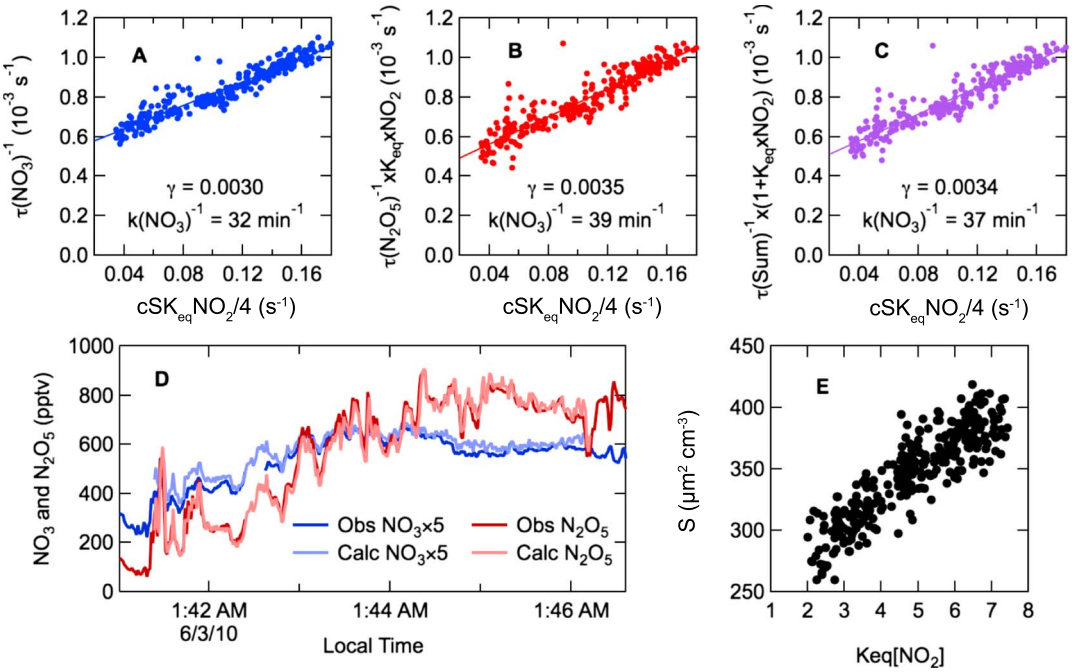

Figure 1. (a–c) Variation of steady state lifetimes with NO_2 and aerosol surface area density (S) together with linear fits to the data. Slopes and intercepts are given by the values of γ_{ss} and $k(NO_3)^{-1}$ shown in each panel and as described in the text. (d) Time series of NO_3 and N_2O_5 data used in Figures 1a–1c, together with calculated steady state NO_3 and N_2O_5 using the parameters derived from the fits in Figures 1a–1c. (e) Variation of S with $K_{eq}[NO_2]$.

$$\tau_{N_2O_5} = \frac{[N_2O_5]}{k[O_3][NO_2]} \tag{13}$$

$$\tau_{sum} = \frac{[NO_3] + [N_2O_5]}{k[O_3][NO_2]} \tag{14}$$

Brown et al. [2009] show that the following identities hold:

$$\tau_{NO_3}^{-1} \approx k_{NO_3} + \frac{1}{4} c_{N_2O_5} S K_{eq}[NO_2]\gamma_{ss} \tag{15}$$

$$\tau_{N_2O_5}^{-1} K_{eq}[NO_2] \approx k_{NO_3} + \frac{1}{4} c_{N_2O_5} S K_{eq}[NO_2]\gamma_{ss} \tag{16}$$

$$\tau_{sum}^{-1} \left(1 + K_{eq}[NO_2]\right) \approx k_{NO_3} + \frac{1}{4} c_{N_2O_5} S K_{eq}[NO_2]\gamma_{ss} \tag{17}$$

Here K_{eq} is the temperature-dependent equilibrium constant of reaction (2), and k_{NO_3} is the first-order loss rate coefficient for the loss of NO_3 to reactions with VOCs. Equations (15)–(17) provide linear relationships with intercept k_{NO_3} and slope γ_{ss} from measurements of mixing ratios of either NO_3, N_2O_5, or the sum, NO_3+N_2O_5. The independent variable is the same in each equation (i.e., $c_{N_2O_5} S K_{eq}[NO_2]/4$) and explicitly accounts for covariance between the mixing ratio of NO_2 (or alternatively the quantity $K_{eq}[NO_2]$) and aerosol surface area density. Note that the aerosol surface area density is corrected to account for aerosol water uptake, as, for example, described in *Brown et al.* [2009]. Although the three measurements are not independent, fits of the data from all three equations provide a check on the consistency of the analysis method. For a derivation of these equations, the reader is referred to *Brown et al.* [2009].

Figure 1 shows an example set of fits for γ_{ss} from a 5.5 min segment of data acquired on a level cruising leg at 800 m above sea level over the eastern Los Angeles Basin on 3 June. Each data point is derived from a set of instantaneously derived quantities.

The three fits in Figures 1a–1c, corresponding to equations (15)–(17), produce individual γ_{ss} values that vary by less than 10% from the average value, and individual k_{NO_3} that vary by less than 12% from the average. The derived k_{NO_3} is consistent with the loss rate coefficient determined by summing the product of VOC concentrations and NO_3 rate coefficients for this flight leg. Figure 1d shows the observed NO_3 and N_2O_5 mixing ratios for these data, together with the NO_3 and N_2O_5 mixing ratios that are calculated from steady state using the derived average k_{NO_3} and γ_{ss}. Figure 1e shows the covariance between S and $K_{eq}[NO_2]$, as described above. There were 10 to 21 determinations for each of the three flights on 29–30 May, 30–31 May, and 3 June. There were no determinations for the 2 June flight because the aerosol size distribution data were not available. We will use these observationally determined uptake coefficients to evaluate the simulated uptake coefficients in section 3.4.

2.4. CalNex 2010 Observations

During CalNex 2010, measurements were taken on aircraft, on a ship, and at ground sites. Since vertical variations in concentration profiles are the focus of this study, model-observation comparisons will mostly use flight measurements by the NOAA P-3 aircraft. Four night flights took place in the Los Angeles Basin. They occurred during a 6 day period, on 29–30 May (evening into the night), 30–31 May (night), 2 June (night to early morning), and 3 June (night to early morning). Measurements on the P-3 relevant to nighttime nitrogen oxide chemistry included NO_2 and O_3 mixing ratios (Chemiluminescence, *Ryerson et al.* [1999] and *Pollack et al.* [2010], and cavity ring down spectroscopy, *Dubé et al.* [2006] and *Wagner et al.* [2011]), NO_3 and N_2O_5 mixing ratios (cavity ring down spectroscopy, *Dubé et al.* [2006] and *Wagner et al.* [2011]), aerosol size distributions (laser particle counter, *Brock et al.* [2003] and *Wilson et al.* [2004]), from which surface area density can be derived, nonrefractory aerosol composition (compact time-of-flight aerosol mass spectrometer, C-ToF-AMS [*Canagaratna et al.*, 2007; *Bahreini et al.*, 2012]) from which submicron aerosol mass concentrations of organic, sulfate, nitrate, ammonium, and chloride are determined, and mixing ratios of speciated volatile organic compounds (VOCs) (whole air samples analyzed by GC-MS, *Schauffler et al.* [1999]) to define the reactivity of NO_3. AMS-measured chloride needs to be considered as a lower limit to what is present in the aerosol phase. The fraction of the reported chloride to total in the sampled plumes was variable; in some plumes, it was as low as 60% while in most others it was greater than 85%. There were also measurements of HNO_3 and $ClNO_2$ mixing ratios, products of heterogeneous N_2O_5 uptake, using chemical ionization mass spectrometry (CIMS) [*Neuman et al.*, 2002; *Slusher et al.*, 2004; *Kercher et al.*, 2009]. The $ClNO_2$ measurements have not been used for the analysis in this paper but have been described elsewhere [*Young et al.*, 2012]. Aerosol size distributions were measured at low relative humidity and corrected for hygroscopic growth as described previously [*Brown et al.*, 2009].

At the ground level, the Los Angeles measurement site was located at the California Institute of Technology in Pasadena (34.140582°N, 118.122455°W, 236 m above sea level). Details on the instrumentation and setup can be found in *Tsai et al.* [2014]. While the site operated from 15 May to 15 June 2010, this study will focus on the dates corresponding to the nighttime flights, 30 May to 2 June 2010.

2.5. WRF-Chem Setup

The host meteorological and air quality model in this study is WRF-Chem, version 3.3.1 [*Grell et al.*, 2005; *Fast et al.*, 2006]. The chosen WRF configuration options for atmospheric processes are listed in Table 1 from *Fast et al.* [2012]. The modeling domain consists of SoCAB, as shown by Figure 2. The model was run using a nested domain with 12 km and 4 km resolution as indicated in Figure 2. The top of the domain vertical coordinate is set at 300 hPa, with 35 vertical layers. The simulation period is the period of 30 May to 3 June 2010, which corresponds to the period when the nighttime flights occurred during CalNex 2010.

We used the CBM-Z chemical mechanism for handling gas-phase reactions [*Zaveri and Peters*, 1999]. This includes the loss pathways of NO_3 due to reaction with a number of VOC species, namely, formaldehyde, acetaldehyde, methylglyoxal, alkenes, phenols, and isoprene. We used the MOSAIC module with eight size bins for partitioning and phase state calculations of the inorganic aerosol [*Zaveri et al.*, 2008]. The aerosol water content, which is an important input parameter for the B&T parameterization, is determined by MOSAIC based on the inorganic aerosol composition and ambient RH using the Zdanovskii-Stokes-Robinson (ZSR) method [*Zdanovskii*, 1948; *Stokes and Robinson*, 1966]. The treatment for organic aerosol is based on the module implemented in PMCAMx [*Gaydos et al.*, 2007] and modified to handle primary species according to recommendations by *Shrivastava et al.* [2008]. The treatment for the N_2O_5 heterogeneous hydrolysis has been described in section 2.2. Lateral boundary conditions were generated using mozbc (http://www.acd.ucar.edu/wrf-chem),

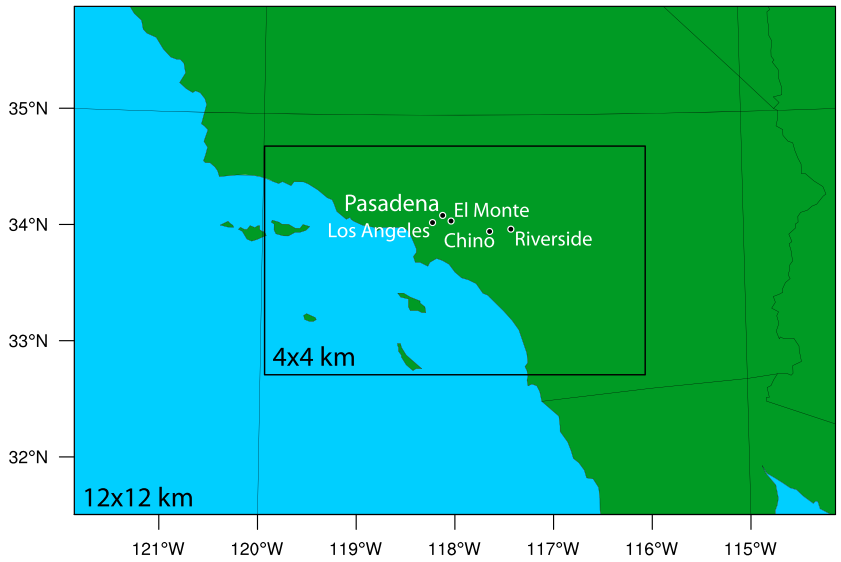

Figure 2. WRF-Chem modeling domain in Southern California, USA.

a preprocessing program that creates time-varying chemical boundary conditions for WRF-Chem from the global Model for Ozone and Related chemical Tracers, version 4 (MOZART-4) output [*Emmons et al.*, 2010]. Initial conditions were developed using mozbc as well, with an additional 48 h spin-up period.

The California Air Resources Board (CARB) 2008 Inventory was the basis for anthropogenic emissions in the model. To capture the decreasing trend in emissions from 2008 to 2010 due to the implementation of air quality regulations and economic downturn, a reduction of 50% was applied to both the gas and aerosol inventories according to the recommendation by *Fast et al.* [2014].

3. Results and Discussion

3.1. Evaluation of Simulated Meteorology and Selected Criteria Pollutants

To demonstrate that the model results are consistent with the conditions during the CalNex campaign, we present comparisons of model results and observations for selected quantities and three locations. The first location is downtown Los Angeles, characterized by coastal weather patterns and fresh emissions of pollutants; the second is Riverside, characterized by high levels of air pollution due to the accumulation of secondary species near the base of the San Jacinto and San Bernardino mountain ranges; and the third is the CalNex ground site in Pasadena.

The comparisons for the meteorological data (wind speed and direction, temperature, and relative humidity) for the three locations are shown in Figures S1 and S2 in the supporting information. These quantities were directly measured at the CalNex ground site in Pasadena. Data for downtown Los Angeles and Riverside were taken from the NOAA National Climatic Data Center (http://www.ncdc.noaa.gov).

For all locations the model captured the diurnal cycles of these quantities well. For the temperature at the CalNex ground site, the bias was 0.95°C with a correlation coefficient of 0.98. For the relative humidity, normalized bias was −20.7%, with a correlation coefficient of 0.92; i.e., the model underpredicted the ground site relative humidity. The model underpredicted relative humidity at nighttime in the inland region such as Riverside as well, with slight overprediction in temperature. The bias for temperature at Los Angeles is −0.05°C, and the correlation coefficient is 0.90. For Riverside, the model has a temperature bias of −0.7°C and the correlation coefficient of 0.96. For relative humidities, the normalized bias and correlation coefficients at Los Angeles are 14% and 0.75, and −1.7% and 0.94 for Riverside, respectively. Biases in simulated relative humidity may have important impacts on the values for uptake coefficients, either directly in the case of the Davis parameterization or indirectly in the case of the B&T parameterization.

Simulated base case concentrations for ozone, NO_x, and particulate matter ($PM_{2.5}$ and PM_{10}) were compared to observations from the CARB Quality Assurance Air Monitoring Sites for Riverside and Los Angeles (CARB, http://www.arb.ca.gov/aqd/aqdcd/aqdcddld.htm) and to observations directly made at the CalNex ground

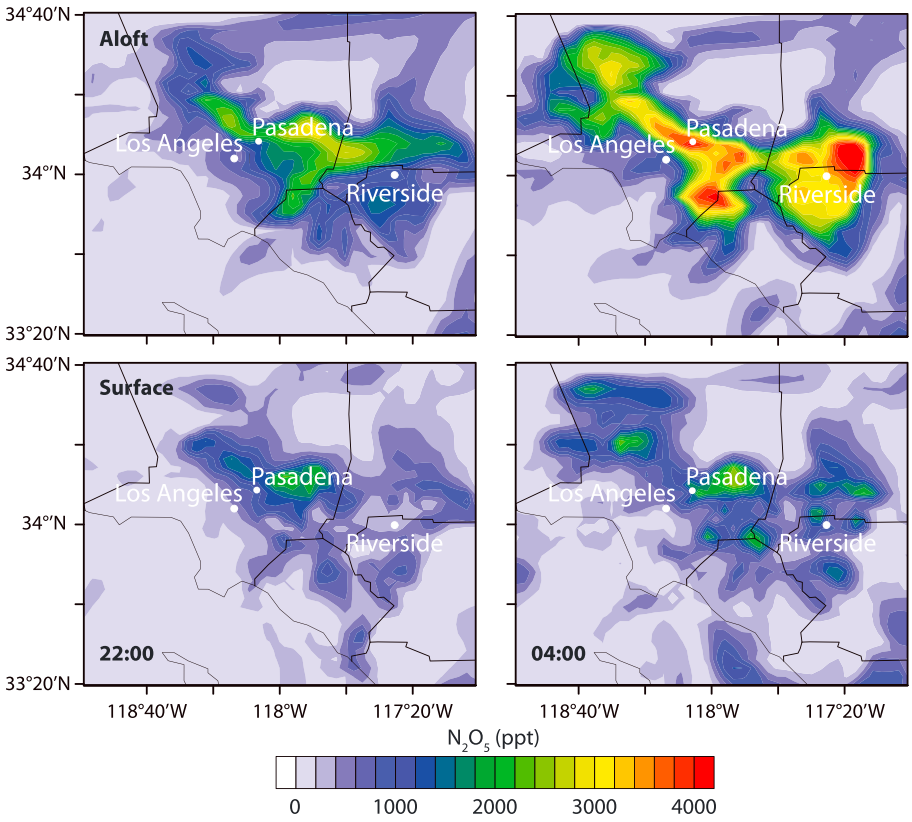

Figure 3. Horizontal spatial distribution of base case modeled N_2O_5 (bottom row) near the surface (below 50 m above ground level (agl)) and (top row) above the stable boundary layer (above 500 m agl) at (left column) 22:00 local solar time (LST) on 31 May and (right column) 04:00 LST on 1 June.

site for Pasadena. The model qualitatively captured the diurnal trends of both gas-phase and aerosol species at all locations (Figures S3 and S4). The model tended to overpredict daytime ozone levels. For Los Angeles, Riverside, and Pasadena the normalized mean biases (NMB) was 58.7%, 20.8%, and 25.0%, respectively. The base case NO_x mixing ratios were also overpredicted at these three locations with NMB of 51.5%, 33.3%, and 98% for Los Angeles, Riverside, and Pasadena, respectively.

It should be noted that the base case simulations did not include the impacts of the heterogeneous hydrolysis of N_2O_5. We will quantify the differences that arise from including the hydrolysis in section 3.6. Including this reaction reduces the average NO_x and O_3 concentrations over the simulation period by up to 3 ppb, thereby improving the model simulations.

3.2. Modeled N_2O_5 Spatial Distributions

This section discusses the simulated distribution of the base case N_2O_5 mixing ratios and is followed by a comparison of the simulated uptake coefficients from the different scenarios listed in Table 1 and their impacts on N_2O_5 vertical profiles (section 3.3).

The spatial distribution of N_2O_5 mixing ratios in the urban atmosphere at night is unique due to the development of the nocturnal boundary layer that decouples emissions from the chemistry in the residual layer. It is therefore helpful to consider the nighttime boundary layer and the residual layer separately. Fresh emissions of NO from mobile sources in SoCAB readily titrate ozone and NO_3, both of which are precursors to N_2O_5. NO_3 also reacts with freshly emitted volatile organic compounds (VOC). Thus, N_2O_5 concentrations are often low within close proximities of emission sources, as illustrated in Figure 3.

For the base case simulation (no hydrolysis), isolated maxima of N_2O_5 mixing ratios developed within the nocturnal boundary layer (Figure 3, bottom row). Based on the model results, the average nocturnal boundary layer height is approximately 500 m above sea level. The number of these "hot spots" increased as the night progressed, but their maximum mixing ratios remained similar in magnitude, around 2.5 ppb. Above

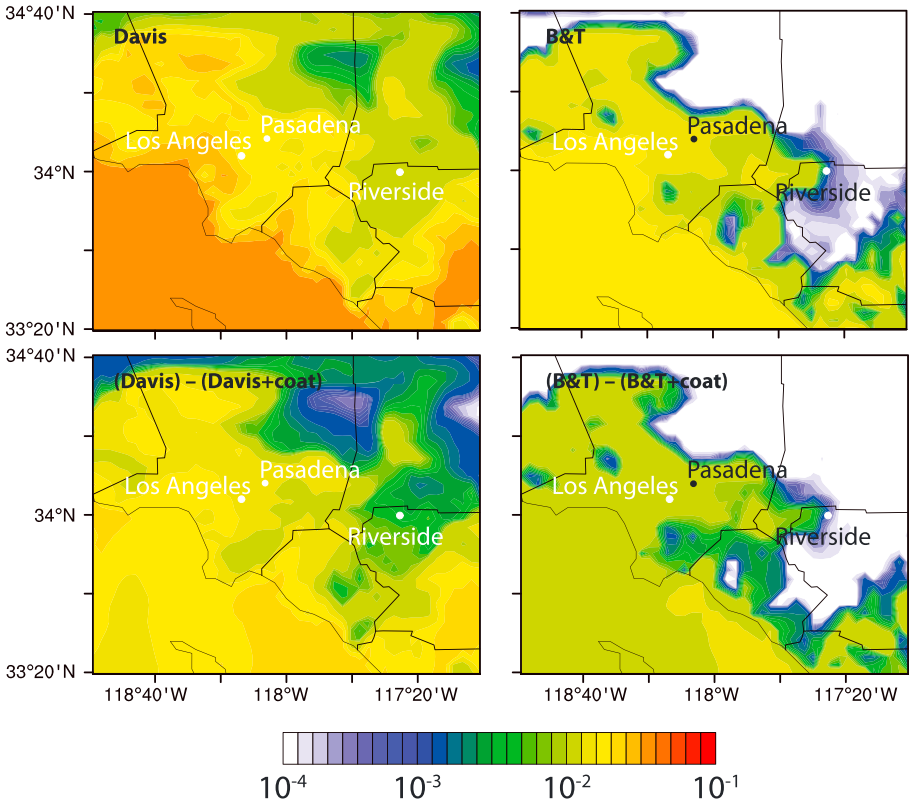

Figure 4. Uptake coefficient in the surface layer for (left column) Davis and (right column) B&T parameterizations (top row) without organic coating treatment (γ_{core}) and (bottom row) absolute differences between uptake coefficients without and with organic coating at 22:00 LST on 31 May.

the nighttime boundary layer, the spatial distribution of N_2O_5 mixing ratios was not directly influenced by the spatial distribution of the emissions as was the case near the surface (Figure 3, top row). Without the constant removal of N_2O_5 precursors, N_2O_5 accumulated in the residual layer (at altitudes greater than 500 m above sea level) during nighttime to values up to 4 ppb.

3.3. Modeled N_2O_5 Uptake Coefficients and Impacts of Hydrolysis on N_2O_5

As described in section 2.2, this study compares and contrasts four different N_2O_5 heterogeneous hydrolysis parameterizations. In this section, we will present how the N_2O_5 uptake coefficients from the four cases listed in Table 1 compare to one another in both the nocturnal boundary layer and the residual layer and how this impacts simulated N_2O_5 mixing ratios.

Figure 4 presents the spatial distribution of γ in the model surface layer for the two aqueous aerosol treatments (Davis and B&T) and the change in γ caused by the inclusion of organic coating (bottom row). To explain the features in the spatial distribution for the individual cases, we discuss this figure in conjunction with Figures 5 and 6, which show the quantities that determine γ, i.e., aerosol nitrate content and RH for the Davis parameterization, aerosol nitrate and water content for the B&T parameterization, and organic aerosol concentration for the coating parameterization. We show the spatial distributions for these quantities at 22:00 local time, but similar findings hold for other hours throughout the night.

The values for the uptake coefficient γ in the surface layer varied by an order of magnitude across the air basin for all cases. The Davis case (Figure 4, top left) showed generally the highest values, with γ^D_{core} approximately 0.06 over the ocean. The values decreased to about 0.005 with increasing distance from the coast. The main factor that explains this spatial pattern in γ^D_{core} was the distribution of RH. The RH values decreased from 90% over the southwest part of the domain to 20% over the northeast (Figure 5, left). As noted in section 2.1, the Davis parameterization includes a RH dependence even for low relative humidity environments with dry aerosol, which *Davis et al.* [2008] explained by the fact that this may be due to an increase in surface-adsorbed water on solid salts as RH increases.

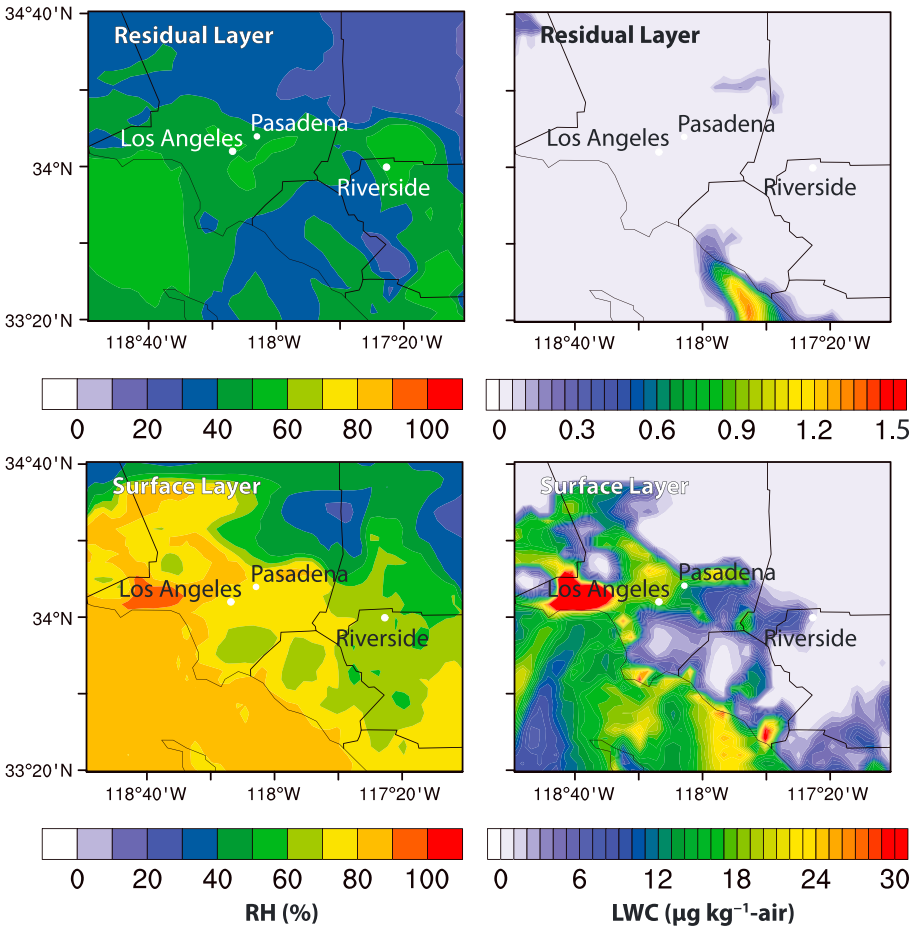

Figure 5. (left column) Base case relative humidities (RH, %) and (right column) aerosol liquid water content (LWC) concentrations (μg kg^{-1}-air) in (bottom row) the surface layer and (top row) the residual layer at 22:00 LST on 31 May.

The highest γ^{B}_{core} values (Figure 4, top right) of 0.04 were also found over the ocean. The spatial distribution of γ^{B}_{core} followed closely the aerosol water content distribution (Figure 5, right). Values of zero for γ^{B}_{core} over the northeastern parts of the domain reflected the absence of water in the aerosol phase at these locations. As mentioned in section 2.5, the thermodynamic model used in WRF-Chem determines the aerosol water content based on the inorganic aerosol composition, and the presence of organic aerosol does not affect the simulated aerosol water content. We also know from section 3.1 that our predictions for ambient RH are biased low. It is therefore likely that our predictions of aerosol water content are biased low, especially at low relative humidity. This, in turn, leads a chemically based parameterization of N_2O_5 uptake such as the B&T parameterization to underestimate the uptake coefficient and highlights that the aerosol thermodynamic models may not accurately capture aerosol liquid water at low RH, rather than a problem with the B&T parameterization itself.

Both γ^{D}_{core} and γ^{B}_{core} also account for uptake inhibition by particulate nitrate. The impact of nitrate suppression can be seen at locations where particulate nitrate dominated over particulate sulfate, such as in the area of east Orange County, southwest of Riverside by the coast (Figure 6, left column).

The organic component in the aerosol also reduces N_2O_5 uptake. The simulated organic coating thicknesses vary with location and time of the day and also for the different size bins. A spatially and temporally averaged value for the organic coating thickness is 3.2 nm. Figure 4 (bottom row) shows the absolute differences between the uptake coefficients without and with coating. A positive value means that the uptake coefficient decreases with coating. Peak values of γ in both the Davis and the B&T cases decreased by a factor of 2, down to 0.03 and 0.02, respectively. The largest reductions in γ due to organic coatings were not necessarily found at locations with the highest concentrations of organics (Figure 6, middle column), but rather at locations

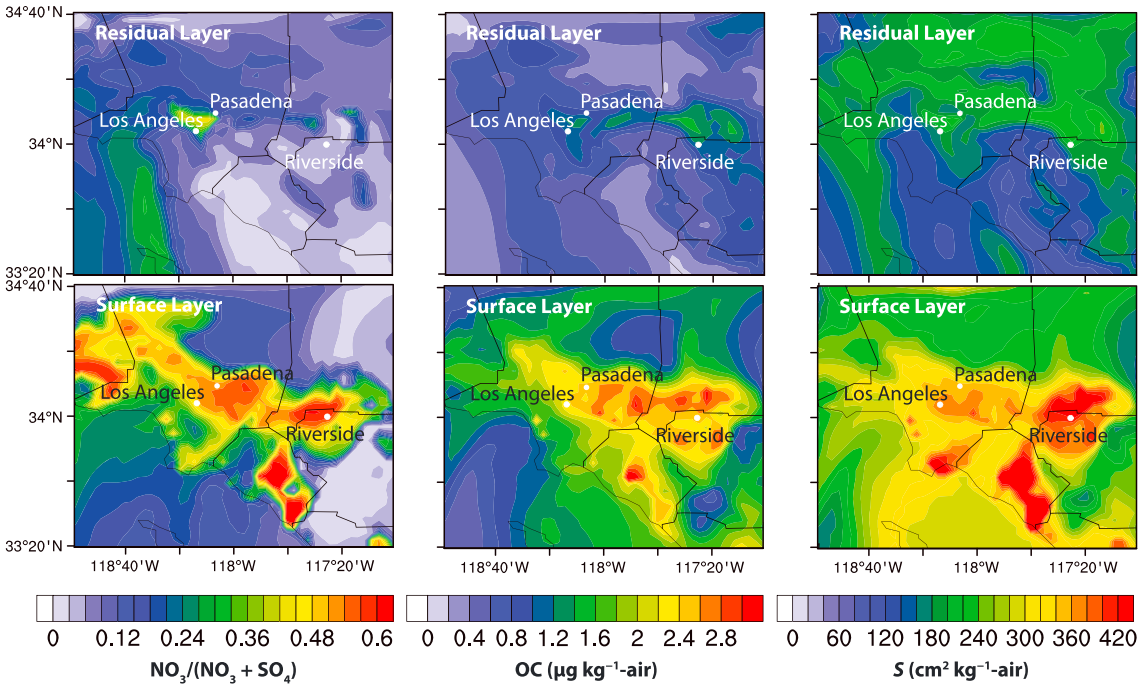

Figure 6. (left column) Particulate nitrate-to-nitrate+sulfate fractions (0 = no nitrates and only sulfates are present; 1 = only nitrates and no sulfates are present); (middle column) organic aerosol concentrations (μg kg^{-1}-air); (right column) aerosol surface area density (*S*, cm^2 kg^{-1}-air) in (bottom row) the surface layer and (top row) the residual layer for the base case at 22:00 LST on 31 May.

where γ_{core} was high, such as in the marine boundary layer and in areas with low nitrate concentrations. This is consistent with *Riemer et al.* [2009] who found that γ is most sensitive to organic coatings when the aerosol nitrate content is low, as shown in their Figure 13.

In the residual layer, γ values are generally lower compared to the surface layer. At altitude 900 m in the model output (Figure 7), γ^{D}_{core} reached maximum values of 0.04 (Figure 7, top left). Lower temperature and lower relative humidities in the residual layer are the causes of the decreasing trend in γ^{D}_{core} with increasing altitude. The Davis parameterization shows a reduction in the N_2O_5 uptake coefficient across the basin where organic material is present in the aerosol phase. For the B&T cases, γ^{B}_{core} reached maximum values of 0.03. The lack of aerosol water again is reflected by near-zero γ^{B}_{core} values, similar to the findings within the nocturnal boundary layer. Given such low value for γ^{B}_{core}, the effects of organic coating are hardly noticeable, as seen in Figure 7 (bottom right).

The reaction rate of N_2O_5 heterogeneous uptake on particles is not only dependent on γ but also on the aerosol surface area density, *S* (equation (6)). Figure 6 (right column) contrasts the spatial distribution of *S* in the surface layer and in the residual layer. The maximum values of *S* were generally found at the surface and were reduced by more than 50% in the residual layer. The highest values of *S* were located near emission sources (Los Angeles) and inland where secondary aerosol forms and accumulates (Riverside). A similar trend and magnitude for the available surface were observed in the aircraft measurements.

Figure 8 shows simulated vertical profiles at 22:00 local time on 31 May over Riverside and Los Angeles. Black lines represent the base case results for N_2O_5 mixing ratios (left) and aerosol surface area density (right); orange and red lines represent the Davis cases with and without organic coating, respectively; green and blue lines represent the B&T cases with and without organic coating, respectively. The base case vertical profile of N_2O_5 mixing ratios has the prominent structure that shows the effects of boundary layer structure that is directly proportional to NO_3 production and reaction rates with VOC. Maximum γ and *S* values are both found within the nocturnal boundary layer, albeit not at the same altitude. Hence, the conditions within the nocturnal boundary layer were more favorable for N_2O_5 heterogeneous uptake than in the residual layer.

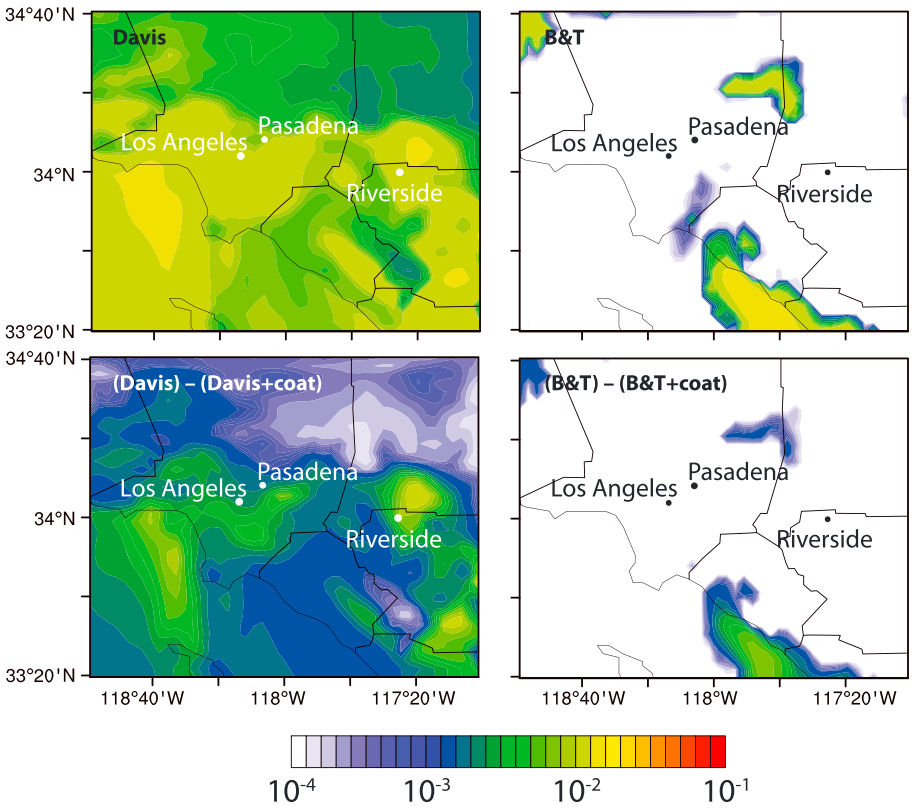

Figure 7. Uptake coefficient in the residual layer for (left column) Davis and (right column) B&T parameterizations (top row) without organic coating treatment (γ_{core}) and (bottom row) changes in γ from Figure 7 (top row) by Riemer organic treatment ($\gamma_{core} - \gamma$) at 22:00 LST on 31 May.

Simulated N_2O_5 mixing ratios are higher in the residual layer than in the nocturnal boundary layer. While the conditions in the residual layer are less favorable for heterogeneous hydrolysis, N_2O_5 mixing ratios are still significantly altered by the uptake process. In the residual layer, relative to the base case, the maximum N_2O_5 mixing ratio is reduced by as much as 90% for the Davis case and 85% for the Davis+coat case. The two B&T cases show a 77% reduction of N_2O_5 due to the heterogeneous hydrolysis reaction relative to the base case. Since γ^B_{core} is already low in the residual layer, the addition of organic coating treatment does not suppress the uptake coefficient by the same magnitude as for the Davis case.

At Riverside, the influence of organic coating on γ^D_{core} is smaller in magnitude than in Los Angeles. Nevertheless, the overall impact of the heterogeneous reaction reduces maximum N_2O_5 mixing ratios by as much as 85% for the Davis case and up to 75% for the Davis+coat case relative to the base case. Values for γ for the two B&T cases (with and without organic coating) are zero for the entire profile (Figure 8, bottom left), preventing hydrolysis to occur for all heights at this location. As discussed previously, this is the result of predicting zero liquid aerosol water content. Although the B&T parameterization does not predict hydrolysis locally, decreases in N_2O_5 mixing ratios from the base case profile are still observed because the heterogeneous hydrolysis impacts at locations upwind from Riverside are propagated by transport.

3.4. Evaluating Closure for Observed and Simulated Uptake Coefficients

Section 2.3 described how N_2O_5 uptake coefficients can be derived based on the steady state analysis introduced by *Brown et al.* [2003]. Here we evaluate closure between γ_{ss} and γ values determined using the parameterizations from section 2.2. As input data for the latter we use (1) aircraft observations, including measurements of aerosol composition with the C-ToF-AMS (Figure 9), and (2) model data from the simulations presented in section 3.3 (Figure 10).

As described in section 2.3, steady state uptake coefficients were derived from observations of the variation of NO_3 and N_2O_5 lifetimes with NO_2 mixing ratio and aerosol surface area density over individual flight segments of 0.5–8 min in duration. Flight segments are numbered sequentially as shown on the *x* axis in Figure 9,

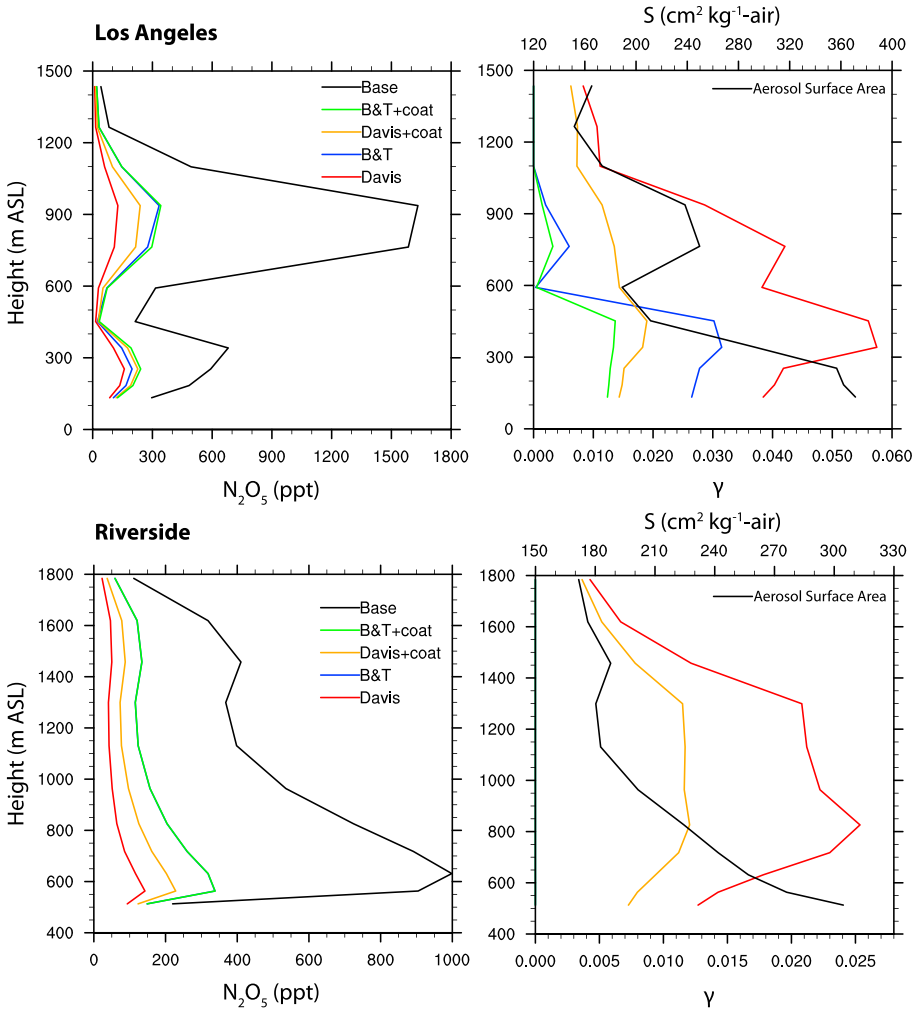

Figure 8. Vertical profiles of (left column) N_2O_5, aerosol surface area density (S, right in black), and (right column) γ at (top row) Los Angeles and (bottom row) Riverside at 22:00 LST on 31 May.

and Figure 9 (left column) shows observed relative humidity and aerosol concentrations of nitrate, sulfate, ammonium, chloride, and organics for the night flights from 30 May and 3 June, averaged over the individual flight segments. We used the same approach as in *Davis et al.* [2008] to determine the amount of ammonium sulfate versus ammonium bisulfate, i.e., we assumed that all of the NO_3^- is present as NH_4NO_3, and the leftover NH_4^+ is distributed between $(NH_4)_2SO_4$ and NH_4HSO_4 according to their equation (11).

These parameters are then used as inputs for the four parameterization cases for γ: Davis, B&T, Davis+coat, and B&T+coat. These same observations are also utilized to estimate the corresponding liquid water content by the E-AIM model (http://www.aim.env.uea.ac.uk/aim/aim.php). We used the E-AIM "Model IV" to predict aerosol water content, which considers the system of H^+, $NH4^+$, Na^+, SO_4^{2-}, NO_3^-, Cl^-, and H_2O [*Friese and Ebel*, 2010], comparable to MOSAIC in WRF-Chem. While it is possible that at least a monolayer of water could persist below the efflorescence point, thereby providing a medium on which N_2O_5 can hydrolyze, we do not account for these effects. Further, to be consistent with the current treatment of aerosol water uptake in WRF-Chem, we do not consider the influence of organics on water uptake.

The results are shown in Figure 9 (right column), together with the uptake coefficients γ_{ss}, which are independently calculated based on steady state analysis for the same flight segments. The relative humidities for the 30 May flight are below 30%, which is below the efflorescence point of the inorganic species mixture present in the aerosol. Hence, E-AIM predicts particles as dry solids for the selected flight segments, resulting in uptake

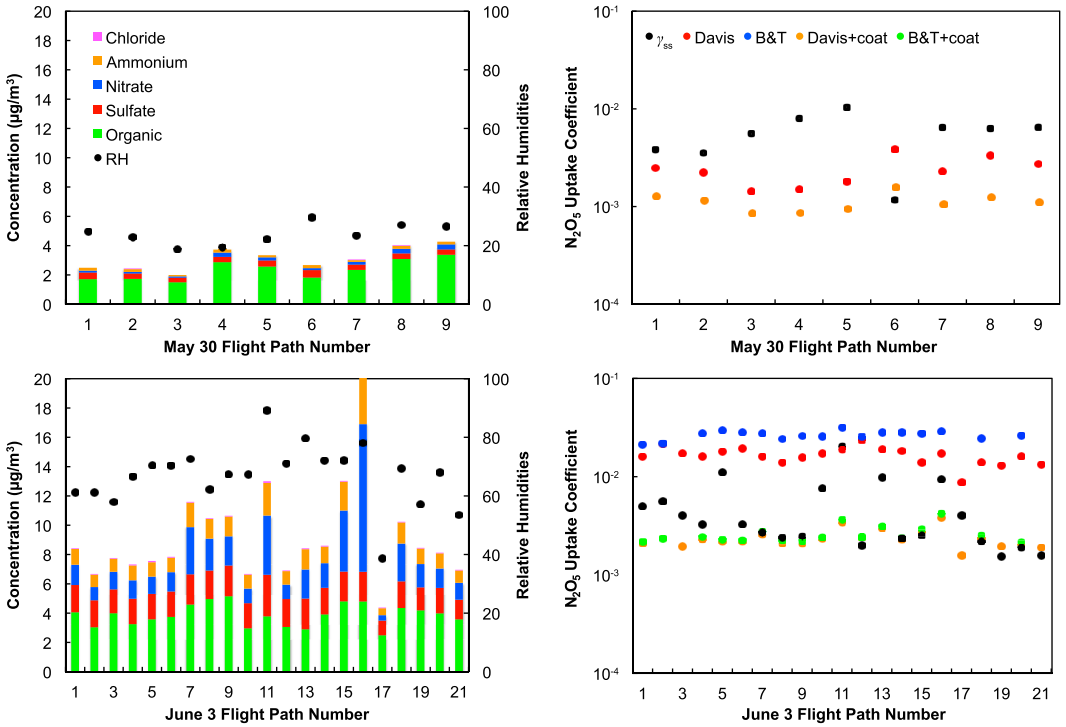

Figure 9. (left column) Averaged ascending/descending flight segment aerosol concentrations and relative humidities. (right column) Uptake coefficients from steady state analysis (γ_{ss}), and from Davis, B&T, Davis+coat, and B&T+coat parameterization methods using aircraft data from (top row) 30 May and (bottom row) 3 June flights as inputs.

coefficients of zero for the B&T parameterization. Again, this is a shortcoming of the method to determine aerosol liquid water content, not of the B&T parameterization itself. The γ values for the Davis and Davis+coat cases for the 30 May flight segments (Figure 9, top row) also underpredict γ_{ss}, by about an factor of 3 without organic coating and by up to an order of magnitude when the organic coating effect is included. This highlights again that low relative humidity environments pose a challenge for aerosol thermodynamic models that are currently used to predict aerosol liquid water content, and this introduces errors in the treatment of the N_2O_5 heterogeneous hydrolysis.

For the flight segments on 3 June, the relative humidities are approximately 70%, and both the Davis and B&T parameterizations yield similar results. The cases without organic coating represent an upper bound,

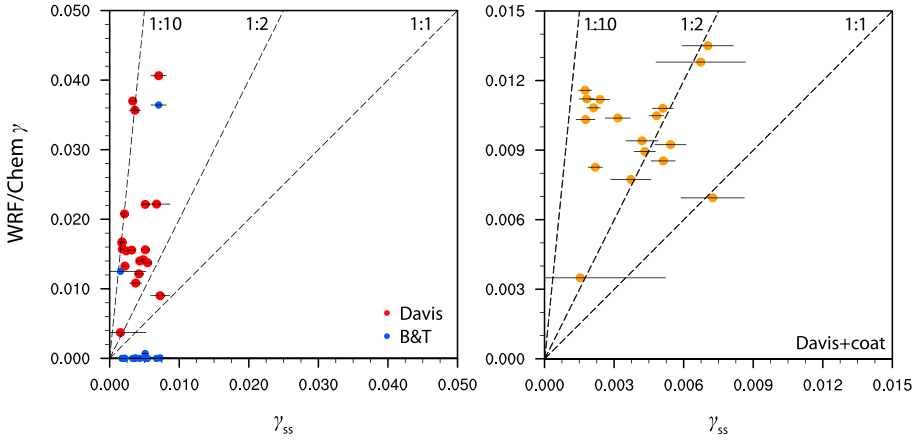

Figure 10. Modeled γ versus calculated γ_{ss} using aircraft observations from the 31 May flight. (left) Davis and B&T parameterization; (right) Davis+coat.

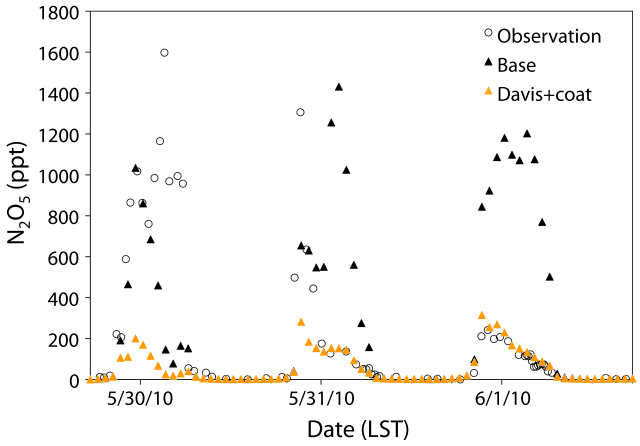

Figure 11. Time series of N_2O_5 DOAS ground site measurements (open circle) from 30 May to 2 June 2010, and corresponding model simulation with no hydrolysis (black) and Davis+coat parameterization (orange). The DOAS measurements are from the layer closest to the surface (33–78 m). The corresponding model results are interpolated to the same average height.

nearly always overpredicting γ_{ss}. Including the organic coating reduces the uptake coefficients by an order of magnitude and results in good closure with γ_{ss}.

Figure 10 shows a comparison γ_{ss} and γ values as determined by the WRF/Chem model simulations. When the impact of organic coatings is not included, γ^{D}_{core} mostly overpredicts observations, while γ^{B}_{core} underpredicts observations (Figure 10, left). The discrepancies between modeled γ^{B}_{core} and γ_{ss} again originate from the same problem of estimating the liquid water content by the model.

When the organic coating treatment is included, the extent of overprediction in γ^{D}_{coat} decreases (Figure 10, note the differences in the scaling of the ordinate between Figure 10 (left) and Figure 10 (right)). While the tendency of overprediction persists even when the organic coating is included, it is a significant improvement from previous works [*Brown et al.*, 2009]. Thus, including the organic coating treatment appears to be essential to achieve closure between modeled and observed uptake coefficient. The current WRF-Chem setup underpredicts the organic component in the aerosol phase, which contributes to the overprediction in γ. At the Pasadena site, observed maximum daily organic aerosol concentrations during the modeling period average around 20 μgm^{-3} [*Hayes et al.*, 2013], while modeled organic aerosol concentrations peak at 5 μgm^{-3}.

3.5. Comparison of Simulated and Observed N_2O_5 Mixing Ratios

Based on the analysis in section 3.4, the Davis+coat parameterization represents best the conditions encountered during the modeling period. For the comparison of modeled N_2O_5 mixing ratios to observations, the focus will therefore be on the Davis+coat case. Figure 11 shows the comparison of simulated diurnal profiles of N_2O_5 mixing ratios at the CalNex 2010 Pasadena ground site for the period of 30 May to 2 June 2010. The observations were taken with differential optical absorption spectroscopy (DOAS) at four height intervals, which were 33–78 m above ground level (agl) for the lowest interval, 78–121 m agl for the middle interval, 121–255 m agl for the upper interval, and 255–556 m agl for the highest intervals. Figure 11 includes the observations from the layer closest to the surface. Corresponding model results are interpolated to the same average height. On 30 May, observed N_2O_5 mixing ratios in the highest interval of up to 1600 ppt (open circle) are greater than even the base case predictions (black triangles, no hydrolysis) that have corresponding low ozone level. On the evenings of 31 May and 1 June, on the other hand, the base case consistently overestimates the observed values while the Davis+coat case (orange triangles) matches the ambient measurements extremely well.

For the assessment of N_2O_5 vertical profiles, measurements from CalNex night flights are compared to model results. Missed approaches were performed during these night flights to capture trace gases throughout the basin. Then, observed concentrations are mapped to the average concentration of the modeling cell that contains the corresponding altitude of the measurement. Figure 12 shows overlays of N_2O_5 flight measurements (purple line), model base case (black line), and model Davis+coat case (orange line) time series for the

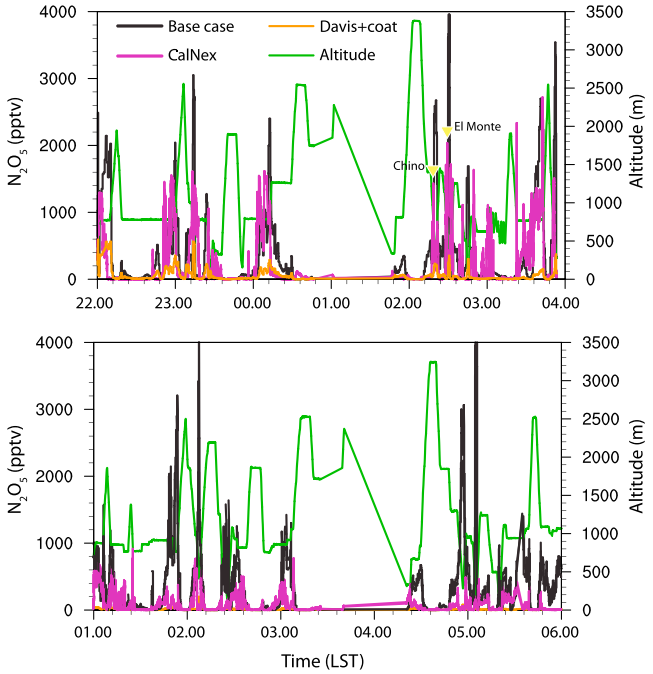

Figure 12. Time series of N_2O_5 flight measurements (purple) from 31 May to (top) 1 June 2010 and (bottom) 2 June 2010 flights, overlaid with the corresponding base case model simulation values, i.e., no inclusion of N_2O_5 heterogeneous hydrolysis (black) and the Davis+coat case (orange).

evening of 31 May to 1 June and early morning on 2 June. Time series of corresponding flight altitudes are also included (green line). For both flights, the model qualitatively captured the major N_2O_5 plumes in the basin. Quantitatively, the base case mostly overpredicted observed N_2O_5 levels, especially for the early morning flight on 2 June.

Looking more closely into individual vertical profiles, two samples of such profiles are shown in Figure 13. Without consideration for heterogeneous hydrolysis (base case), the model consistently overpredicted N_2O_5 mixing ratios by a factor of 2 or more. This confirms the necessity of including the heterogeneous hydrolysis to model N_2O_5. When the Davis+coat heterogeneous hydrolysis parameterization was included, modeled N_2O_5 levels agreed with observations higher up in the residual layer where N_2O_5 concentrations were low (above 1200 m in Chino and above 800 m in El Monte). Just above the nocturnal boundary, however, higher levels of N_2O_5 were observed than the model predicted. Two issues can contribute to this. First, as shown in Figure 10, γ^{D}_{coat} values are higher than the observed γ values; hence, the underprediction of N_2O_5 is expected. Second, the vertical resolution decreases with increasing altitude in WRF-Chem leading to a lower spatial resolution in the residual layer (where most of the flight measurements were taken) compared to the surface layer. The larger cell volume in model layers at a high altitude may lead to artificial averaging of N_2O_5. Also, the effects of diminished N_2O_5 levels through averaging can propagate throughout the whole domain, making it difficult to distinguish local contributions from domain-wide trends.

3.6. Impacts of the Heterogeneous Hydrolysis of N_2O_5 on Ozone and NO_x

Lastly, we quantified the impact of Davis+coat heterogeneous N_2O_5 hydrolysis parameterization on mixing ratios of criteria pollutant levels over the simulation period (31 May to 2 June 2010) at three particular monitoring sites (Los Angeles, Pomona, and Riverside) (Table 2). Los Angeles is closest to the coastline, Riverside is inland near the edge of the air basin, and Pomona is in between the two. Pollutant emissions rates are high in Los Angeles, so primary pollutants are expected to dominate the species composition, especially when onshore winds are present. Hence, the highest mixing ratios of NO_x and low ozone levels were found in Los Angeles. When moving eastward from Los Angeles to inland toward Riverside, the shift from fresh to aged pollutants was evident in the decrease in NO_x levels and the increase in ozone mixing ratios. At Riverside, pollutants accumulated near the base of the mountain ranges, and some of the highest levels of secondary

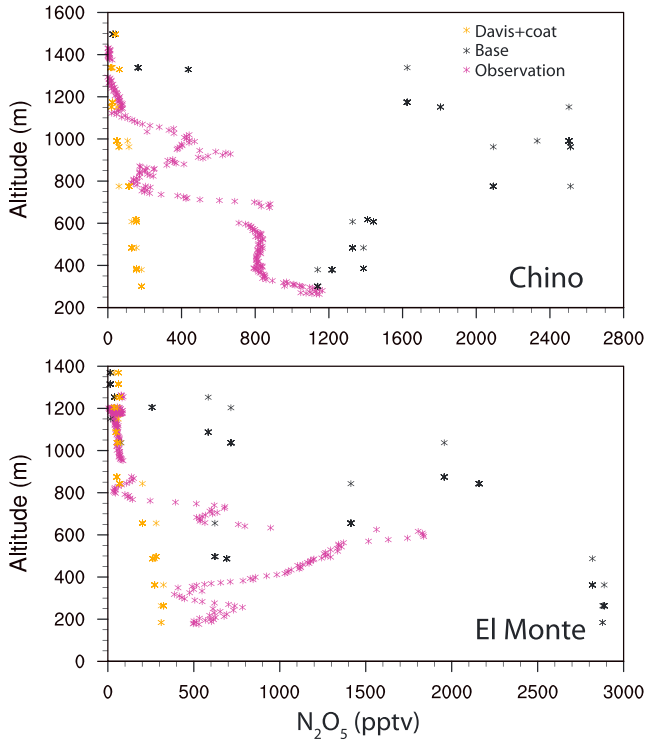

Figure 13. Vertical profiles of N_2O_5 at (top) Chino and (bottom) El Monte from CalNex observations (purple) and predictions by the base case (black) and the Davis+coat case (orange).

pollutants (e.g., ozone) across the basin were found here. As shown in Table 2, the model was able to capture these NO_x and ozone trends for Los Angeles, Pomona, and Riverside with positive correlation values, with the performance improving going inland. The base case model results consistently overpredicted NO_x mixing ratios across the air basin, and including the N_2O_5 heterogeneous hydrolysis process improved the model performance by reducing the NO_x budget at night that can be carried over into the daytime. *Tsai et al.* [2014] drew similar conclusions on the importance of nighttime NO_x loss mechanisms in polluted environments. Quantitatively, the inclusion of the heterogeneous hydrolysis improved predicted average ozone and NO_x mixing ratios by up to 10% and 33%, respectively.

Table 2. Model Evaluation Metrics Over the Simulation Period, 31 May to 2 June 2010: Modeled and Observed Values Show Averages (Range) in ppb, Normalized Mean Bias (NMB) and Normalized Mean Error (NME) are in Percentage, and Root-Mean-Square Error (RMSE) is in ppb

Case	Species	Site	Modeled (ppb)	Observed (ppb)	NMB	NME	RMSE	*r*	*n*
Base	Ozone	Los Angeles	61 (1.5–84)	38 (20–66)	58.7	65.7	28	0.49	31
Davis+coat	Ozone	Los Angeles	58 (1.2–81)	38 (20–66)	51.1	58.9	25	0.54	31
Base	Ozone	Pomona	64 (37–88)	45 (13–73)	44.5	48.3	25	0.61	28
Davis+coat	Ozone	Pomona	63 (35–87)	45 (13–73)	40.9	44.8	23	0.65	28
Base	Ozone	Riverside	64 (26–88)	53 (12–86)	20.8	30.6	19	0.67	30
Davis+coat	Ozone	Riverside	63 (23–87)	53 (12–86)	18.4	28.5	18	0.70	30
Base	NO_x	Los Angeles	24 (14–68)	15 (7–41)	51.5	58.0	13	0.49	31
Davis+coat	NO_x	Los Angeles	22 (14–64)	15 (7–41)	38.9	52.0	12	0.38	31
Base	NO_x	Pomona	13 (5–29)	15 (7–61)	−11.2	55.1	11	0.39	28
Davis+coat	NO_x	Pomona	11 (5–22)	15 (7–61)	−25.9	51.3	12	0.30	28
Base	NO_x	Riverside	13 (4–38)	10 (4–35)	33.3	50.0	7	0.74	30
Davis+coat	NO_x	Riverside	10 (4–30)	10 (4–35)	5.4	44.8	6	0.70	30

4. Conclusions

We implemented the N_2O_5 heterogeneous hydrolysis parameterizations according to *Davis et al.* [2008] ("Davis"), *Bertram and Thornton* [2009] ("B&T"), and *Riemer et al.* [2009] ("+coat") into the WRF-Chem model. Four test scenarios were developed: Davis, Davis+coat, B&T, and B&T+coat. In general, for all cases modeled N_2O_5 uptake coefficients on particles, γ, were higher near the surface, especially over marine and coastal areas where relative humidities were high.

The model predicted little or no aerosol water content in the residual layer, leading to a significant low bias in the B&T parameterization, which is based on liquid water content, rather than relative humidity. In this study, uptake coefficients calculated using the B&T parameterization tended to be nearly zero in the residual layer. This contradicts the observations, which documented heterogeneous hydrolysis to occur everywhere across the air basin during CalNex. We emphasize that this should not be interpreted as a failure of the B&T parameterization. Rather, the results highlight the need for better thermodynamic models to predict aerosol water uptake, in particular at low ambient RH. Similar issues with the B&T parameterization sensitivity to relative humidity predictions were also suggested by *Lowe et al.* [2014].

Overall, the Davis+coat case best captured observed γ values, and improved the comparison to observed N_2O_5 mixing ratios, as it was evident from comparison with observations made at the CalNex ground site. Including the impacts of organic coating was crucial to reduce the overprediction of simulated γ values. However, even after taking the coating into account, the model still overestimated γ values. This may be attributed to the underprediction of the organic aerosol budget by the model. It should also be noted that the organic coating treatment is rather simple as it does not take into account any dependence on relative humidity as suggested by *Grzinic et al.* [2015]. Despite these shortcomings, the Davis+coat parameterization improved the model performance in predicting surface mixing ratios of ozone and NO_x, through the reduction of the tropospheric NO_x budget buildup at night carried into the daytime.

Acknowledgments
We would like to thank Charles Brock for providing his measurement data for our analysis, the NOAA Atmospheric Chemistry, Climate and Carbon Cycle Program, and the California Air Resources Board for funding (ARB 08-318). The data used are listed in the references, and model output data can be obtained by contacting N. Riemer (nriemer@illinois.edu) or W. Chang (wlchang@illinois.edu).

References

Aldener, M., et al. (2006), Reactivity and loss mechanisms of NO_3 and N_2O_5 in a polluted marine environment: Results from in situ measurements during New England Air Quality Study 2002, *J. Geophys. Res.*, *111*, D23S73, doi:10.1029/2006JD007252.

Anttila, T., A. Kiendler-Scharr, R. Tillmann, T. F. Mentel (2006), On the reactive uptake of gaseous compounds by organic-coated aqueous aerosols: Theoretical analysis and application to the heterogeneous hydrolysis of N2O5, *J. Phys. Chem. A*, *110*(35), 10,435–10,443.

Bahreini, R., et al. (2012), Gasoline emissions dominate over diesel in formation of secondary organic aerosol mass, *Geophys. Res. Lett.*, *39*, L06805, doi:10.1029/2011GL050718.

Bertram, T. H., and J. A. Thornton (2009), Toward a general parameterization of N_2O_5 reactivity on aqueous particles: The competing effects of particle liquid water, nitrate and chloride, *Atmos. Chem. Phys.*, *9*, 8351–8363.

Brock, C. A., et al. (2003), Particle growth in urban and industrial plumes in Texas, *J. Geophys. Res.*, *108*(D3), 4111, doi:10.1029/2002JD002746.

Brown, S. S., H. Stark, and A. R. Ravishankara (2003), Applicability of the steady state approximation to the interpretation of atmospheric observations of NO_3 and N_2O_5, *J. Geophys. Res.*, *108*(D17), 4539, doi:10.1029/2003JD003407.

Brown, S. S., et al. (2006), Variability in nocturnal nitrogen oxide processing and its role in regional air quality, *Science*, *311*(5757), 67–70, doi:10.1126/science.1120120.

Brown, S. S., et al. (2007a), Vertical profiles in NO_3 and N_2O_5 measured from an aircraft: Results from the NOAA P-3 and surface platforms during the New England Air Quality Study 2004, *J. Geophys. Res.*, *112*, D22304, doi:10.1029/2007JD008883.

Brown, S. S., W. P. Dubé, H. D. Osthoff, D. E. Wolfe, W. M. Angevine, and A. R. Ravishankara (2007b), High resolution vertical distributions of NO_3 and N_2O_5 through the nocturnal boundary layer, *Atmos. Chem. Phys.*, *7*(1), 139–149, doi:10.5194/acp-7-139-2007.

Brown, S. S., et al. (2009), Reactive uptake coefficients for N_2O_5 determined from aircraft measurements during the Second Texas Air Quality Study: Comparison to current model parameterizations, *J. Geophys. Res.*, *114*, D00F10, doi:10.1029/2008JD011679.

Brown, S. S., et al. (2011), Budgets for nocturnal VOC oxidation by nitrate radicals aloft during the 2006 Texas Air Quality Study, *J. Geophys. Res.*, *116*, D24305, doi:10.1029/2011JD016544.

Canagaratna, M., et al. (2007), Chemical and microphysical characterization of ambient aerosols with the aerodyne aerosol mass spectrometer, *Mass Spectrom. Rev.*, *26*(2), 185–222, doi:10.1002/mas.20115.

Chang, W. L., P. V. Bhave, S. S. Brown, N. Riemer, J. Stutz, and D. Dabdub (2011), Heterogeneous atmospheric chemistry, ambient measurements, and model calculations of N_2O_5: A review, *Aerosol Sci. Technol.*, *45*, 665–695, doi:10.1080/02786826.2010.551672.

Davis, J. M., P. V. Bhave, and K. M. Foley (2008), Parameterization of N_2O_5 reaction probabilities on the surface of particles containing ammonium, sulfate, and nitrate, *Atmos. Chem. Phys.*, *8*, 5295–5311.

Dentener, F. J., and P. J. Crutzen (1993), Reaction of N_2O_5 on tropospheric aerosols: Impact on the global distributions of NO_x, O_3, and OH, *J. Geophys. Res.*, *98*(D4), 7149–7163, doi:10.1029/92JD02979.

Dubé, W. P., S. S. Brown, H. D. Osthoff, M. R. Nunley, S. J. Ciciora, M. W. Paris, R. J. McLaughlin, and A. R. Ravishankara (2006), Aircraft instrument for simultaneous, in situ measurement of NO_3 and N_2O_5 via pulsed cavity ring-down spectroscopy, *Rev. Sci. Instruments*, *77*(3), 34101, doi:10.1063/1.2176058.

Emmons, L. K., et al. (2010), Description and evaluation of the Model for OZone And Related chemical Tracers, version 4 (MOZART-4), *Geosci. Model Dev.*, *3*(1), 43–67, doi:10.5194/gmd-3-43-2010.

Evans, M. J., and D. J. Jacob (2005), Impact of new laboratory studies of N_2O_5 hydrolysis on global model budgets of tropospheric nitrogen oxides, ozone and OH, *Geophys. Res. Lett.*, *32*, L09813, doi:10.1029/2005GL022469.

Fast, J. D., W. I. Gustafson, R. C. Easter, R. A. Zaveri, J. C. Barnard, E. G. Chapman, G. A. Grell, and S. E. Peckham (2006), Evolution of ozone, particulates, and aerosol direct radiative forcing in the vicinity of Houston using a fully coupled meteorology-chemistry-aerosol model, *J. Geophys. Res.*, *111*, D21305, doi:10.1029/2005JD006721.

Fast, J. D., et al. (2012), Transport and mixing patterns over Central California during the Carbonaceous Aerosol and Radiative Effects Study (CARES), *Atmos. Chem. Phys.*, *12*(4), 1759–1783, doi:10.5194/acp-12-1759-2012.

Fast, J. D., et al. (2014), Modeling regional aerosol and aerosol precursor variability over California and its sensitivity to emissions and long-range transport during the 2010 CalNex and CARES campaigns, *Atmos. Chem. Phys.*, *14*, 10,013–10,060, doi:10.5194/acp-14-10013-2014.

Friese, E., and A. Ebel (2010), Temperature dependent thermodynamic model of the system H^+-$NH4^+$-Na^+-SO_4^{2-}-NO_3^--Cl^--H_2O, *J. Phys. Chem. A*, *114*(43), 11,595–11,631, doi:10.1021/jp101041j, pMID: 21504090.

Galmarini, S., P. G. Duynkerke, and J. V.-G. de Arellano (1997), Evolution of nitrogen oxide chemistry in the nocturnal boundary layer, *J. Appl. Meteorol.*, *36*, 943–957, doi:10.1175/1520-0450(1997)036<0943:EONOCI>2.0.CO;2.

Gaydos, T. M., R. Pinder, B. Koo, K. M. Fahey, G. Yarwood, and S. N. Pandis (2007), Development and application of a three-dimensional aerosol chemical transport model, PMCAMx, *Atmos. Environ.*, *41*, 2594–2611, doi:10.1016/j.atmosenv.2006.11.034.

Geyer, A., and J. Stutz (2004), Vertical profiles of NO_3, N_2O_5, O_3, and NO_x in the nocturnal boundary layer: 2. Model studies on the altitude dependence of composition and chemistry, *J. Geophys. Res.*, *109*, D12307, doi:10.1029/2003JD004211.

Grell, G. A., S. E. Peckham, R. Schmitz, S. A. McKeen, G. Frost, W. C. Skamarock, and B. Eder (2005), Fully coupled "online" chemistry within the WRF model, *Atmos. Environ.*, *39*(37), 6957–6975, doi:10.1016/j.atmosenv.2005.04.027.

Grzinic, G., A. Türler, and M. Ammann (2015), Viscosity controls humidity dependence of N_2O_5 uptake to citric acid aerosol, *Atmos. Chem. Phys.*, *15*, 13615–13625, doi:10.5194/acp-15-13615-2015.

Hanway, D., and F.-M. Tao (1998), A density functional theory and ab initio study of the hydrolysis of dinitrogen pentoxide, *Chem. Phys. Lett.*, *285*(5–6), 459–466, doi:10.1016/S0009-2614(97)01382-1.

Hayes, P. L., et al. (2013), Organic aerosol composition and sources in Pasadena, California, during the 2010 CalNex campaign, *J. Geophys. Res. Atmos.*, *118*, 9233–9257, doi:10.1002/jgrd.50530.

Kane, S. M., F. Caloz, M.-T. Leu (2001), Heterogeneous uptake of gaseous N2O5 by (NH4)2SO4, NH4HSO4, and H2SO4 aerosols, *J. Phys. Chem. A*, *105*, 6465–6470.

Kercher, J. P., T. P. Riedel, and J. A. Thornton (2009), Chlorine activation by N_2O_5: Simultaneous, in situ detection of $ClNO_2$ and N_2O_5 by chemical ionization mass spectrometry, *Atmos. Meas. Tech.*, *2*(1), 193–204, doi:10.5194/amt-2-193-2009.

Kim, Y. J., S. N. Spak, G. R. Carmichael, N. Riemer, and C. O. Stanier (2014), Modeled aerosol nitrate formation pathways during wintertime in the great lakes region of North America, *J. Geophys. Res. Atmos.*, *119*, 12,420–12,445, doi:10.1002/2014JD022320.

Lowe, D., et al. (2014), WRF-Chem model predictions of the regional impacts of N_2O_5 heterogeneous processes on nighttime chemistry over north-western Europe, *Atmos. Chem. Phys.*, *15*, 1385–1409, doi:10.5194/acpd-15-1385-2015.

Macintyre, H. L., and M. J. Evans (2010), Sensitivity of a global model to the uptake of N_2O_5 by tropospheric aerosol, *Atmos. Chem. Phys.*, *10*(15), 7409–7414, doi:10.5194/acp-10-7409-2010.

Mielke, L. H., A. Furgeson, and H. D. Osthoff (2011), Observation of $ClNO_2$ in a mid-continental urban environment, *Environ. Sci. Technol.*, *45*, 8889–8896, doi:10.1021/es201955u.

Morgan, W. T., et al. (2015), Influence of aerosol chemical composition on N_2O_5 uptake: Airborne regional measurements in northwestern Europe, *Atmos. Chem. Phys.*, *15*(2), 973–990, doi:10.5194/acp-15-973-2015.

Neuman, J. A., et al. (2002), Fast-response airborne in situ measurements of HNO_3 during the Texas 2000 Air Quality Study, *J. Geophys. Res.*, *107*, 4436, doi:10.1029/2001JD001437.

Pathak, R. K., T. Wang, and W. S. Wu (2011), Nighttime enhancement of $PM_{2.5}$ nitrate in ammonia-poor atmospheric conditions in Beijing and Shanghai: Plausible contributions of heterogeneous hydrolysis of N_2O_5 and HNO_3 partitioning, *Atmos. Environ.*, *45*, 1183–1191, doi:10.1016/j.atmosenv.2010.09.003.

Phillips, G. J., M. J. Tang, J. Thieser, B. Brickwedde, G. Schuster, B. Bohn, J. Lelieveld, and J. N. Crowley (2012), Significant concentrations of nitryl chloride observed in rural continental Europe associated with the influence of sea salt chloride and anthropogenic emissions, *Geophys. Res. Lett.*, *39*, L10811, doi:10.1029/2012GL051912.

Pollack, I., B. Lerner, and T. Ryerson (2010), Evaluation of ultraviolet light-emitting diodes for detection of atmospheric NO_2 by photolysis—Chemiluminescence, *J. Atmos. Chem.*, *65*(2–3), 111–125, doi:10.1007/s10874-011-9184-3.

Riedel, T. P., T. H. Bertram, O. S. Ryder, S. Liu, D. A. Day, L. M. Russell, C. J. Gaston, K. A. Prather, and J. A. Thornton (2012), Direct N_2O_5 reactivity measurements at a polluted coastal site, *Atmos. Chem. Phys.*, *12*, 2959–2968, doi:10.5194/acp-12-2959-2012.

Riemer, N., H. Vogel, B. Vogel, B. Schell, I. Ackermann, C. Kessler, and H. Hass (2003), Impact of the heterogeneous hydrolysis of N_2O_5 on chemistry and nitrate aerosol formation in the lower troposphere under photosmog conditions, *J. Geophys. Res.*, *108*(D4), 4144, doi:10.1029/2002JD002436.

Riemer, N., H. Vogel, B. Vogel, T. Anttila, A. Kiendler-Scharr, and T. Mentel (2009), The relative importance of organic coatings for the heterogeneous hydrolysis of N_2O_5, *J. Geophys. Res.*, *114*, D17307, doi:10.1029/2008JD011369.

Russell, A. G., G. J. McRae, and G. R. Cass (1985), The dynamics of nitric acid production and the fate of nitrogen oxides, *Atmos. Environ.*, *19*(6), 893–903, doi:10.1016/0004-6981(85)90234-3.

Ryerson, T. B., et al. (2013), The 2010 California research at the Nexus of air quality and climate change (CalNex) field study, *J. Geophys. Res. Atmos.*, *118*, 5830–5866, doi:10.1002/jgrd.50031.

Ryerson, T. B., L. G. Huey, K. Knapp, J. A. Neuman, D. D. Parrish, D. T. Sueper, and F. C. Fehsenfeld (1999), Design and initial characterization of an inlet for gas-phase NO_y measurements from aircraft, *J. Geophys. Res.*, *104*(D5), 5483–5492, doi:10.1029/1998JD100087.

Sarwar, G., H. Simon, P. Bhave, and G. Yarwood (2012), Examining the impact of heterogeneous nitryl chloride production on air quality across the United States, *Atmos. Chem. Phys.*, *12*, 6455–6473, doi:10.5194/acp-12-6455-2012.

Sarwar, G., H. Simon, J. Xing, and R. Mathur (2014), Importance of tropospheric $ClNO_2$ chemistry across the northern hemisphere, *Geophys. Res. Lett.*, *41*, 4050–4058, doi:10.1002/2014GL059962.

Schauffler, S. M., E. L. Atlas, D. R. Blake, F. Flocke, R. A. Lueb, J. M. Lee-Taylor, V. Stroud, and W. Travnicek (1999), Distributions of brominated organic compounds in the troposphere and lower stratosphere, *J. Geophys. Res.*, *104*(D17), 21,513–21,535, doi:10.1029/1999JD900197.

Shrivastava, M. K., T. E. Lane, N. M. Donahue, S. N. Pandis, and A. L. Robinson (2008), Effects of gas particle partitioning and aging of primary emissions on urban and regional organic aerosol concentrations, *J. Geophys. Res.*, *113*, D18301, doi:10.1029/2007JD009735.

Slusher, D. L., L. G. Huey, D. J. Tanner, F. M. Flocke, and J. M. Roberts (2004), A Thermal Dissociation-Chemical Ionization Mass Spectrometry (TD-CIMS) technique for the simultaneous measurement of peroxyacyl nitrates and dinitrogen pentoxide, *J. Geophys. Res.*, *109*, D19315, doi:10.1029/2004JD004670.

Stokes, R. H., and R. A. Robinson (1966), Interaction in aqueous nonelectrolyte solution. Part I: Solute-solvent equilibria, *J. Phys. Chem.*, *70*, 2126–2130.

Stutz, J., B. Alicke, R. Ackermann, A. Geyer, A. White, and E. Williams (2004), Vertical profiles of NO_3, N_2O_5, O_3, and NO_x in the nocturnal boundary layer: 1. Observations during the Texas Air Quality Study 2000, *J. Geophys. Res.*, *109*, D12306, doi:10.1029/2003JD004209.

Thornton, J. A., et al. (2010), A large atomic chlorine source inferred from mid-continental reactive nitrogen chemistry, *Nature*, *464*(7286), 271–274, doi:10.1038/nature08905.

Tsai, C., et al. (2014), Nocturnal loss of NO_x during the 2010 CalNex-LA study in the Los Angeles Basin, *J. Geophys. Res.*, *119*, 13,004–13,025, doi:10.1002/2014JD022171.

Wagner, N. L., W. P. Dubé, R. A. Washenfelder, C. J. Young, I. B. Pollack, T. B. Ryerson, and S. S. Brown (2011), Diode laser-based cavity ring-down instrument for NO_3, N_2O_5, NO, NO_2 and O_3 from aircraft, *Atmos. Meas. Tech.*, *4*(6), 1227–1240, doi:10.5194/amt-4-1227-2011.

Wagner, N. L., et al. (2012), The sea breeze/land breeze circulation in Los Angeles and its influence on nitryl chloride production in this region, *J. Geophys. Res*, *117*, D00V24, doi:10.1029/2012JD017810.

Wilson, J. C., B. G. Lafleu, H. Hilbert, W. R. Seebaugh, J. Fox, D. W. Gesler, C. A. Brock, B. J. Huebert, and J. Mullen (2004), Function and performance of a low turbulence inlet for sampling supermicron particles from aircraft platforms, *Aerosol Sci. Technol.*, *38*(8), 790–802, doi:10.1080/027868290500841.

You, Y., et al. (2012), Images reveal that atmospheric particles can undergo liquid-liquid phase separations, *Proc. Natl. Acad. Sci.*, *109*(33), 13,188–13,193, doi:10.1073/pnas.1206414109.

Young, C. J., et al. (2012), Vertically resolved measurements of nighttime radical reservoirs in Los Angeles and their contribution to the urban radical budget, *Environ. Sci. Technol.*, *46*, 10,965–10,973, doi:10.1021/es302206a.

Zaveri, R. A., and L. K. Peters (1999), A new lumped structure photochemical mechanism for large-scale applications, *J. Geophys. Res.*, *104*, 30,387–30,415, doi:10.1029/1999JD900876.

Zaveri, R. A., R. C. Easter, J. D. Fast, and L. K. Peters (2008), MOdel for Simulating Aerosol Interactions and Chemistry (MOSAIC), *J. Geophys. Res.*, *113*, D13204, doi:10.1029/2007JD008782.

Zdanovskii, A. B. (1948), New methods of calculating solubilities of electrolytes in multicomponent systems, *Z. Fiz. Khim.*, *22*, 1475–1485.